REVISTA MATÉRIA V.29 N.3
ISSN 1517-7076 articles e20240339, 2024

An investigation of strain measurement on curved surface using photogrammetry with validation

Thiyagarajan Prabaharan[1], Pitchaipillai Periyasamy[1], Venu Mugendiran[2]

[1]St Peter's Institute of Higher Education and Research, Department of Mechanical Engineering. 600054, Chennai, Tamilnadu, India.

[2]Anna University, Madras Institute Technology Campus, Department of Production Technology. 600044, Chromepet, Tamilnadu, India.

e-mail: prabaezhile1977@gmail.com, psamy75@gmail.com, mugendiran.v@mitindia.edu

ABSTRACT

Metal forming is a crucial technique for shaping sheet material to specific dimensions. Predicting strain in formed components is essential for evaluating sheet metal formability. This study investigates the measurement of major and minor strain on curved surfaces formed through a single-point incremental forming process using photogrammetry and validates the results. The aim is to measure strain on a curved surface post-forming by applying circle grids on the sheet metal before forming. A system was developed to capture deformed circle grids and compare the deformation with the original diameter to calculate strain. A Forming Limit Diagram was plotted to analyze the formability of the sheet metal. Statistical methods were used to predict the confidence interval level of the developed strain. The average percentage error of the strain obtained through 3D photogrammetry method compared to the experimental results is approximately 1.91% and 2.93% for the major and minor axes, respectively. These findings demonstrate that photogrammetry analysis of strain on curved surfaces is more accurate than traditional experimental methods.

Keywords: Incremental forming; Circle grid analysis; Strain measurement; Photogrammetry.

1. INTRODUCTION

Sheet metal forming is widely used in various industrial sectors such as automotive, aerospace, home appliances, and food industries due to its exceptional strength, superior surface quality and precise tolerances. To assess the formability of sheet metals, various techniques are employed including mechanical testing, simulations, limiting dome height measurements and forming limit diagrams [1, 2]. Studies has been found utilizing digital volume reconstruction technique on electrodes through focussed ion beam to study the porosity and tortuosity of the electrodes [3–5]. Traditional methods for measuring strain, such as mylar tapes, microscopes and ruler are time consuming process and provide results with low resolution [6]. Automated methods for measuring dimensions have been developed to determine strains more efficiently [7]. Strain distribution measurements on formed parts are essential for assessing product quality, evaluating material formability and validating forming process simulations [8]. Contactless optic measurements are often used to evaluate stress in drawn components by analysing pre-etched texture pattern that change during the forming process [9, 10]. Advanced technologies and software, such as computer vision, digital image correlation, and laser interferometry, offer precise strain measurement capabilities but require significant financial resources [11]. Photogrammetry provides advantages over single point strain gauges by offering 3D full field strain data for homogenous, non-homogenous, and anisotropic materials [12]. This method allows for the observations of regions with significant strain gradients and enables direct comparison to finite element analysis results, potentially reducing the need for prototypes [13]. Researchers have utilized photogrammetry for studying plastic strain in deep drawing and evaluating automobile body fabrication [14]. A simplified workflow with high accuracy and repeatability was developed for conducting 3D photogrammetry on human bones of varying sizes and geometry to create photorealistic reconstructions within allowed standard deviations for quantitative analysis in anatomy education [15]. Photogrammetric data was used to reconstruct degraded cemented soil samples to characterize surface roughness parameters and predict the relationship between tensile strength and roughness parameters [16]. An automated auxiliary measuring equipment based on photogrammetry was developed to inspect flange faces on a multi-branch welded tube by

Corresponding Author: Thiyagarajan Prabaharan Received on 07/06/2024 Accepted on 24/07/2024

DOI: https://doi.org/10.1590/1517-7076-RMAT-2024-0339

capturing high-performance images and employing an in-plane rotating structure for precise measurements [17]. A digital measuring setup utilizing photogrammetry techniques was created to study erosion by digitizing eroded sand particles in the micron range flowing through a pipeline into 3D models for analyzing hydrodynamic characteristics, erosion rate, and collision angles at pipe bends [18]. Fracture toughness of a cast iron sample was determined using a 3D photogrammetry setup by tracking crack mouth opening displacement through a three-point bending method, with the corner radius of the crack opening as the reference point for deformation measurement [19]. An innovative methodology using Photonic Clustered Regularly Interspaced Short Palindromic Repeat (CRISPR) with optical sensors and plasmon resonance was employed to measure the sensitivity of SARS-CoV-2 variants, including Omicron, in 'positive' samples for accurate target detection [20]. A unique approach combining DNA origami probes and surface plasmon resonance biosensors was introduced for diagnosing early-stage lung cancer by determining the level of mutation in the KRAS gene on circular tumor DNAs [21]. Photogrammetry-based 3D scanning has become a cost-effective option for early-stage product design with advancements in digital cameras, computers, and algorithms, making it a viable alternative to traditional 3D scanning equipment [22]. This study aims to test the feasibility of using low-cost 3D scanning with a single digital camera in physical prototyping and digitalization, particularly for smaller-scale applications, and focuses on the development of an automated strain measurement system. Images captured by the camera of the formed surface were analyzed to determine strain using the Digital Image Correlation method [23–25]. The low-cost image capturing setup and processing method can be used to study strain in any forming process.

2. MATERIALS AND METHODOLOGY

2.1. Materials

Incremental forming, a promising method primarily used for prototyping, was utilized in this study. The key advantage of this process is the elimination of tool and die costs associated with traditional forming methods. A single-point hemispherical tool followed a predetermined spiral path generated by a CNC program to shape the fixed sheet metal to the desired dimensions. Localized deformation occurs on the desired path due to single point contact between the tool and the sheet metal. Advantage of this process, if needed the programme can be modified immediately according to the requirement. A vertical machining center was employed for this operation. Aluminum alloy 5052 series sheet metal with a thickness of 1 mm was selected for the study. Table 1 displays the chemical composition of AA5052 sheet metal.

Formability is primarily determined by the material's ability to stretch without fracturing [26]. The uniaxial tension test measures the material's deformation capacity before fracturing. Tensile test specimens were prepared according to ASTM E8/E8M standards and subjected to deformation. The obtained data on load vs. Displacement allowed for the determination of the material's elastic limit, ultimate tensile strength, strain hardening exponent, strength coefficient, and percentage of elongation [27, 28]. The sheet metal's hardness was predicted using a brinell hardness tester. The predicted mechanical properties were tabulated and presented in Table 2.

2.2. Methodology

Circles with a diameter of 6 mm and a pitch of 10 mm between their centers were etched using a laser etching machine. The depth of the circles was maintained at 1 μm. Figure 1 depicts the laser machine and the etched surface of the sheet metal that will undergo deformation.

Table 1: AA5052 alloy chemical composition.

COMPOSITION	MG	CR	SI	FE	CU	MN	ZN	AL
Nominal	2.23	0.18	0.14	0.31	0.01	0.05	0.001	Rem
Actual	2.18 – 2.78	0.14 – 0.33	0.0 – 0.23	0.0 – 0.38	0.08	0.08	0.08	Rem

Table 2: AA5052 alloy mechanical properties.

YIELD STRENGTH (MPA)	ULTIMATE TENSILE STRENGTH (MPA)	PERCENTAGE OF ELONGATION	STRENGTH COEFFICIENT (MPA)	STRAIN HARDENING EXPONENT	MODULUS OF ELASTICITY (MPA)	BRINELL HARDNESS (BHN)
243	272	13	290	0.211	70	61

The tool material for single point incremental forming process was selected as high-speed steel tool.

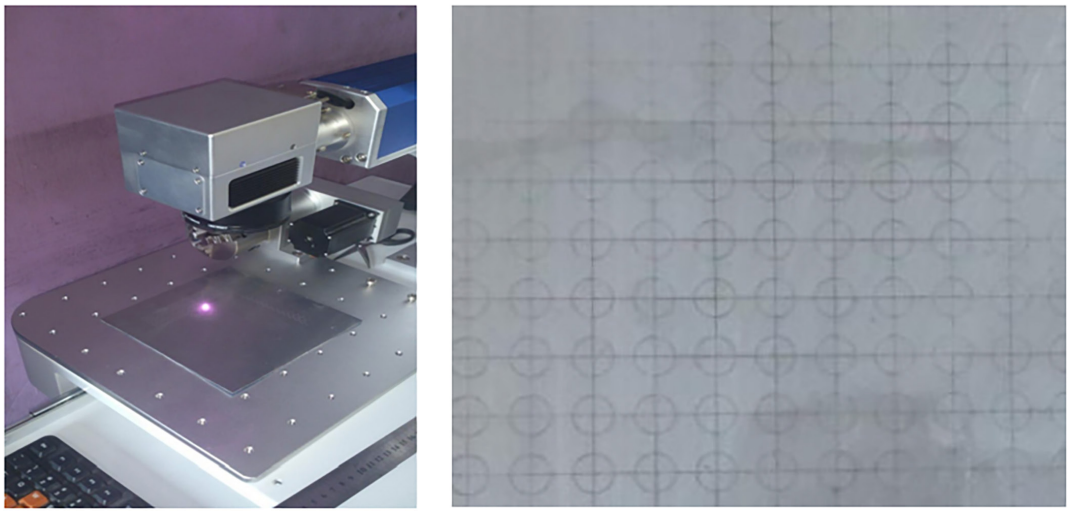

Figure 1: Laser etching machine and the etched surface.

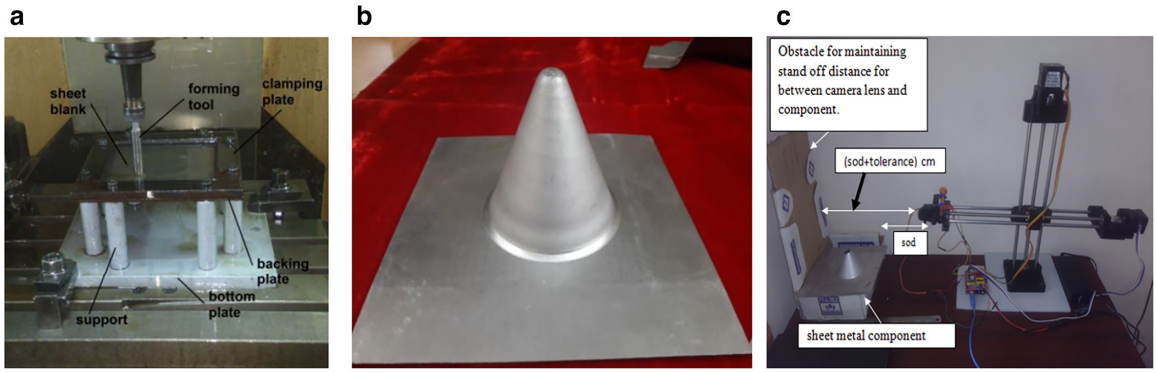

Figure 2: (a) & (b) Fixture along with sheet metal and formed component. (c) Setup to measure the strain on the surface of the formed component.

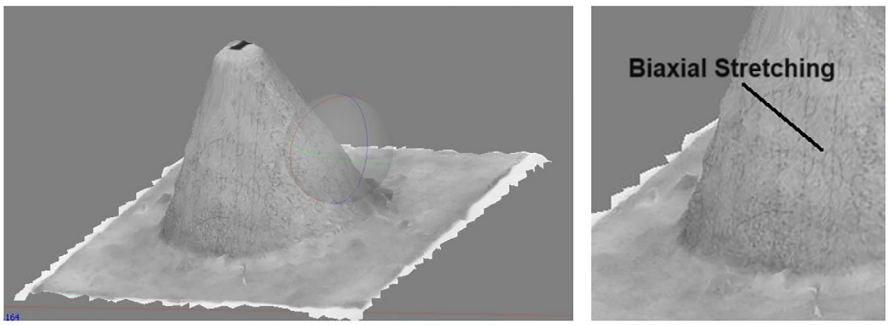

Figure 3: Reconstructed Image of the formed component and biaxial stretching on the surface of the component.

The etched sheet metal was secured in a specialized fixture designed for the incremental forming process. A hemispherical tool made of HSS followed a predetermined spiral path created using a numerical control program to form a cone with a 70 mm diameter and a wall angle of 65°. The forming parameters for incremental forming were set as follows: spindle speed at 1500 rpm, tool feed at 500 rpm, and step depth at 0.25 mm. The fixture, along with the fixed sheet metal and the formed component, is depicted in the Figure 2.

The setup for acquiring deformation of the circle through the photogrammetry process is illustrated in Figure 3. The strain measurement setup includes components such as a flexible stand for freely moving the camera, a rotatable table with motorized control for rotating the component 360 degrees, an ultrasonic sensor, a linear actuator with a stepper motor, an Allied Vision Stingray F-201B/F-201C Camera, a Sharp IR

sensor (GP2Y0A21), a servo motor, an Arduino UNO Mega 2560 microcontroller, and a Stepper Motor Driver (DRV8825).

3. RESULTS AND DISSCUSSION

3.1. Image reconstruction

The dataset is prepared for photogrammetry by capturing continuous images with a consistent stand-off distance (SOD). The resolution of the 3D reconstructed picture depends on the number of images provided to the software program. Agisoft 3D reconstruction software utilizes the triangulation algorithm in the photogrammetry process to compare and identify matching points in the images, connecting them to generate point clouds. Meshroom software is then employed to mesh the data and filter out undesired points and environmental data. The reconstructed image is depicted in the Figure 3. Errors may occur during image capturing due to improper camera positioning, inaccuracies in the principal distance between the camera and the measurement surface, camera intersection angles, and lens distortion caused by camera resolution. Also, there is a crucial difficulty in capturing the rotating objects or surfaces in 3D photogrammetry. Another challenge relies on highly reflective surfaces. To minimize lens distortion, it is important to know the internal parameters and settings of the camera and use a fully calibrated camera for orientation with a CMOS setup. Reducing the standoff distance between the camera and the surface being measured can help reduce the impact of intersecting angles. Implementing a minimum of three-point distance feedback system can help reduce inaccuracies in the principal distance between the camera and the surface being captured. The challenge of capturing moving surfaces can be overcome by understanding matching points and utilizing software capabilities effectively. For reflective surfaces, masking or painting can be used, along with proper lighting to reduce reflections.

3.2. Image reconstruction

The high-definition camera captured an image that was converted to binary format. Background noise was eliminated from the binary image, and centroids of closed regions were detected after filtering. Strain was calculated based on the movement of major and minor axes. The specimen was initially photographed in 3-channel RGB and then converted to a single-channel grayscale image. Each pixel in the colored image contains three values ranging from 0 (black) to 255 (white) representing red, blue, and green. Since the color of a pixel is the sum of its three colors, it cannot be directly converted to binary. To address this, the image was converted to grayscale, where each pixel represents an intensity value between 0 and 255. The grayscale image was then transformed to binary by setting a threshold based on the intensity level. In the binary image, pixel values are either 0 (black) or 1 (white). The dataset obtained through photogrammetry for strain calculation is shown in the Figure 4.

The strain calculation was performed using the Zephyr 3D photogrammetry system. The 2D image of the component was converted into a 3D structure, as illustrated in the Figure 5. From the 3D images of the component, the diameters of circles and ellipses (representing strain) on curved, irregular, or bent surfaces can be measured. These surfaces are more susceptible to necking and cracks, making it crucial to measure strain in addition to 2D surfaces. After subjecting the sheet metal to strain, the circles deform into different ellipses. The major and minor axis diameters are used to determine the strain for each circle on the component. The measurements for the deformed ellipses were shown in the Figure 5. These measurements were conducted using the 3D Zephyr photogrammetry software.

Figure 4: Data set for photogrammetry method for strain measurement.

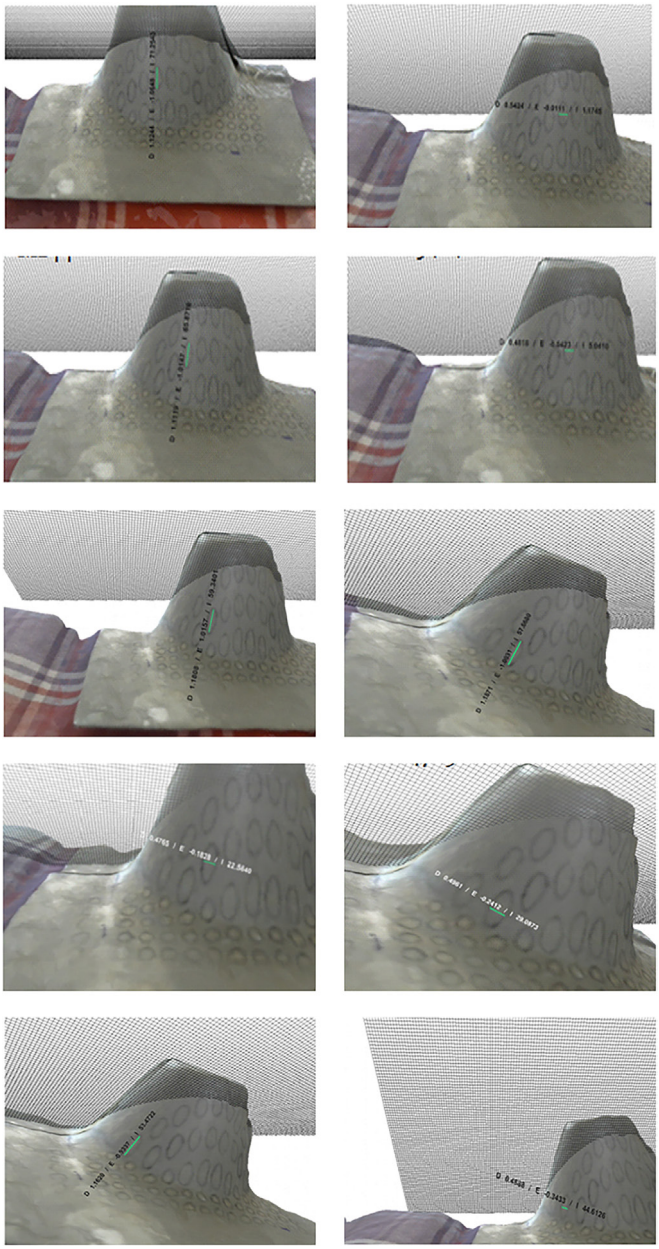

Figure 5: Deformation data of deformed circle obtained for photogrammetry.

The major and minor strains were calculated from the major and minor axis diameters obtained through photogrammetry using the following equations:

$$Major\ Strain = \frac{change\ of\ diameter\ in\ major\ axis}{original\ diameter\ of\ the\ circle} = \frac{d_1 - d_0}{d_0} \quad (1)$$

$$Minor\ Strain = \frac{change\ of\ diameter\ in\ minor\ axis}{original\ diameter\ of\ the\ circle} = \frac{d_2 - d_0}{d_0} \quad (2)$$

where d_1 – change in major diameter, d_2 – change in minor diameter and d_0 – original diameter.

The same formula was used to calculate the major and minor strains developed on the surface of the formed component. A flexible tape with deformed circles printed on it was used for manual calculation, as shown in the Figure 6. The deformed circles' major and minor axes on the tape were matched with the original ones on the surface of the component, and the major and minor diameter values were obtained.

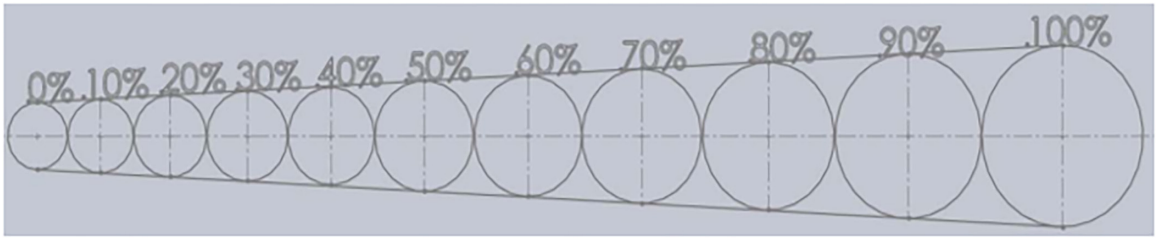

Figure 6: Flexible ruler used for measuring the deformed circles.

Table 3: Strain comparison between the experimental results and photogrammetry analysis.

ELLIPSE NO.	EXPERIMENTAL RESULTS		PHOTOGRAMMETRY		% OF ERROR	
	MAJOR STRAIN	MINOR STRAIN	MAJOR STRAIN	MINOR STRAIN	MAJOR STRAIN	MINOR STRAIN
1.	0.773	0.327	0.7981	0.3362	3.2471	2.8135
2.	0.727	0.314	0.7433	0.3214	2.2421	2.3567
3.	0.823	0.353	0.8355	0.3646	1.5188	3.2861
4.	0.641	0.286	0.6567	0.2948	2.4493	3.0769
5.	0.775	0.353	0.7849	0.3741	1.2774	5.9773
6.	0.885	0.412	0.9222	0.4323	4.2034	4.9272
27.	0.547	0.187	0.5654	0.1875	3.3638	0.2674
8.	0.635	0.243	0.6416	0.2617	1.0394	7.6955
9.	0.757	0.322	0.7778	0.3359	2.7477	4.3168
10.	0.865	0.353	0.8691	0.3542	0.4740	0.3399
11.	0.542	0.213	0.5593	0.2284	3.1919	7.2300
–	–	–	–	–	–	–
–	–	–	–	–	–	–
23.	0.623	0.273	0.6386	0.2646	2.5040	−3.0769
24.	0.747	0.327	0.7548	0.3498	1.0442	6.9725
25.	0.847	0.353	0.8661	0.3691	2.2550	4.5609
26.	0.515	0.202	0.5213	0.1893	1.2233	−6.2871
27.	0.603	0.279	0.5985	0.2655	−0.7463	−4.8387
–	–	–	–	–	–	–
–	–	–	–	–	–	–
34.	0.726	0.313	0.7357	0.3227	1.3361	3.0990
35.	0.808	0.343	0.7999	0.3559	−1.0025	3.7609
36.	0.307	0.113	0.3222	0.1212	4.9511	7.2566
37.	0.473	0.153	0.4944	0.1644	4.5243	7.4510
38.	0.573	0.197	0.5886	0.2086	2.7225	5.8883
39.	0.687	0.257	0.7028	0.2478	2.2999	−3.5798
40.	0.768	0.285	0.7651	0.2881	−0.3776	1.0877
41.	0.535	0.142	0.5413	0.1533	1.1776	7.9577
42.	0.636	0.168	0.6375	0.1695	0.2358	0.8929
–	–	–	–	–	–	–
–	–	–	–	–	–	–

The calculated values of the major and minor strain were tabulated and shown in the following Table 3.

Using the above the forming limit diagram was plotted between major and minor strain and shown below.

The formability of sheet metal can be predicted using a Forming Limit Diagram (FLD), which displays major and minor strains on the y and x axes. Figure 7 shows the predicted FLD with an approximate 45° positive slope, indicating equibiaxial stretching and an increase in major strain leading to an increase in minor strain

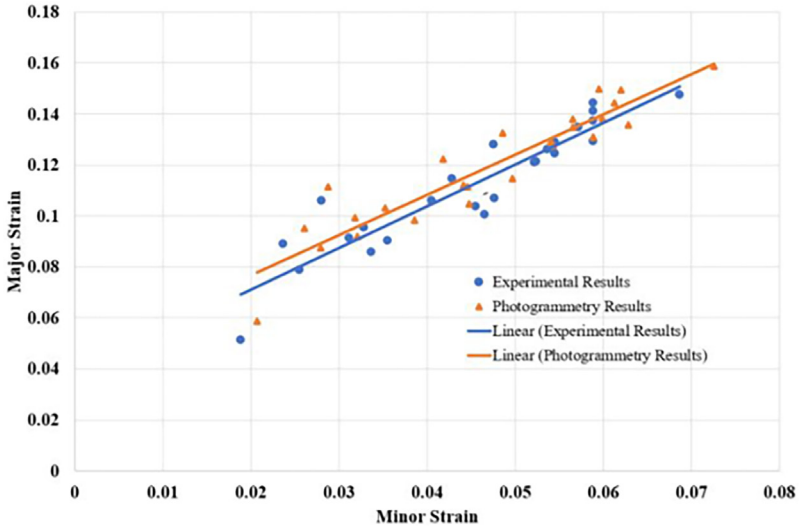

Figure 7: Predicted forming limit diagram.

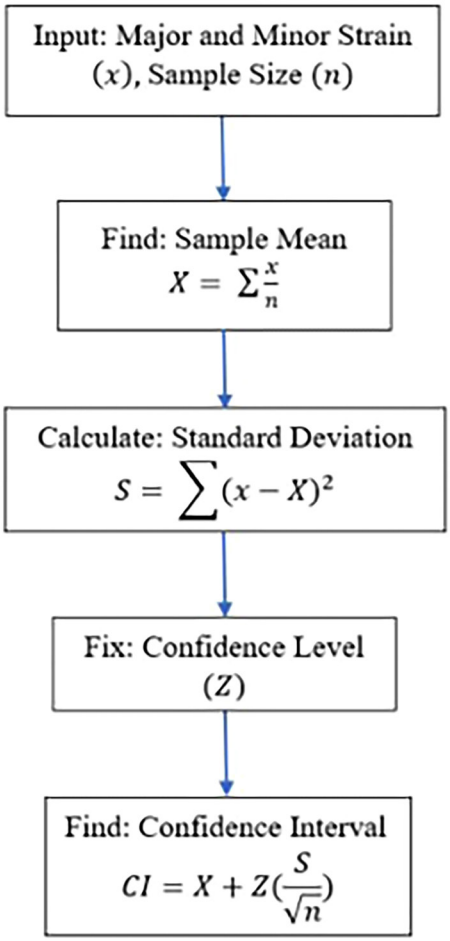

Figure 8: Flow chart describing the confidential interval calculation.

(major strain ≈ minor strain), suggesting the involvement of plastic strain during forming. The Figure 7 also indicates that the strain measured using 3D photogrammetry has high accuracy compared to traditional methods.

3.3. Statistical analysis

The confidence interval is a statistical measure that provides a range of values within which the true mean is likely to fall, along with the level of certainty associated with this estimate. Figure 8, below outlines the steps for calculating the confidence level. The confidence interval is crucial in statistical analysis as it shows the range of probability for results to fall around the sample mean, indicating the level of certainty or uncertainty in the results of surveys or studies. Calculating the confidence interval helps determine the confidence level, which is the percentage of certainty. Statisticians often use a confidence level of 95% to 99% to ensure consistent results when repeating a study. The following flow chart indicates the process flow in calculating the confidence interval. The 95% confidence interval for the data is 0.26998 to 0.67631.

4. CONCLUSIONS

During the forming process, sheet metal undergoes plastic deformation, which can lead to fractures. Analyzing the strain resulting from this deformation is crucial for preventing fractures. In this study, strain on the curved surface of a component formed through single-point incremental forming was analyzed using photogrammetric techniques. A low-cost setup with a camera mounted on an arm capable of moving in three directions was utilized, along with sensors to maintain a constant distance between the surface and the camera. Zephyr software was employed to determine the diameter of deformed circles. Manual measurements of strain on the surface were also taken using a flexible tape and tabulated. The Forming Limit Diagram plotted indicates equibiaxial stretching, meaning that as the major strain increases, the minor strain also increases on a curved surface through single-point incremental forming. A comparison between manual calculations and data from the photogrammetric technique was conducted to determine the percentage of accuracy achieved by photogrammetry. The percentage of error when compared with the 3D photogrammetric technique ranged between 1.91% and 2.93%. A statistical method was used to determine the confidence interval, which was found to be between 0.26998 and 0.67631 at a 95% confidence level. The results demonstrated that the accuracy increased with the image processing method, indicating that the low-cost setup can be used for rapid calculation of strain deformation on curved surfaces.

5. BIBLIOGRAPHY

[1] EVLEN, H., KADI, İ., YAŞAR, M., "Effects of die corner radius and temperature on the formability of AA7075-T6 alloy", *Acta Metallurgica Sinica*, v. 26, n. 5, pp. 623–629, 2013. doi: http://doi.org/10.1007/s40195-013-0129-5.

[2] KIM, S.B., HUH, H., BOK, H.H., *et al*., "Forming limit diagram of auto-body steel sheets for high-speed sheet metal forming", *Journal of Materials Processing Technology*, v. 211, n. 5, pp. 851–862, 2011. doi: http://doi.org/10.1016/j.jmatprotec.2010.01.006.

[3] SARUR, B.J.M., CIDADE, R.A., BRAGA, V.P., *et al*., "Volume reconstruction of SOFC electrode for porosity and tortuosity calculation", *Revista Materia.*, v. 18, n. 1, pp. 67–74, 2013.

[4] PACIORNIK, S., D'ALMEIDA, J., "Digital microscopy and image analysis applied to composite materials characterization", *Matéria*, v. 15, n. 2, pp. 172–181, 2010. doi: http://doi.org/10.1590/S1517-70762010000200013.

[5] MANOJ, M., KRISHNAN, G., MUGENDIRAN, V., "Effect of conventional and microwave sintering on microstructural and mechanical properties of AA7075/SiC/ZrC hybrid MMCs through powder metallurgy route", *Revista de Matemáticas*, v. 28, n. 4, e20230230, 2023.

[6] SAFAEI, M., DE WAELE, W., HERTSCHAP, K., "Characterization of deep drawing steels using optical strain measurements", *Steel Research International*, v. 4, pp. 403–406, 2012, http://hdl.handle.net/1854/LU-3004846, accessed in August, 2024.

[7] ZHANG, D.H., WANG, M.Y., LI, Y.Q., "A challenge for strain optical measurement for bimetal", *Advanced Materials Research*, v. 382, pp. 392–395, 2012. doi: http://doi.org/10.4028/www.scientific.net/AMR.382.392.

[8] SHI, B.Q., LIANG, J., "Circular grid pattern based surface strain measurement system for sheet metal forming", *Optics and Lasers in Engineering*, v. 50, n. 9, pp. 1186–1195, 2012. doi: http://doi.org/10.1016/j.optlaseng.2012.04.007.

[9] STOUGHTON, T.B., YOON, J.W., "A new approach for failure criterion for sheet metals", *International Journal of Plasticity*, v. 27, n. 3, pp. 440–459, 2011. doi: http://doi.org/10.1016/j.ijplas.2010.07.004.

[10] MA, N., TAKADA, K., SATO, K., "Measurement of local strain path and identification of ductile damage limit based on simple tensile test", *Procedia Engineering*, v. 81, pp. 1402–1407, 2014. doi: http://doi.org/10.1016/j.proeng.2014.10.164.

[11] EMBLOM, W.J., JONES, R.J., AITHAL, M., *et al*., "The development of a microscale strain measurement system applied to sheet bulge hydroforming", *Journal of Manufacturing Processes*, v. 16, n. 2, pp. 320–328, 2014. doi: http://doi.org/10.1016/j.jmapro.2014.02.001.

[12] ČINÁK, M., SCHREK, A., ŽITŇANSKÝ, P., "Plastic strain measurments of deep drawn part by means of photogrammetry", *Scientific Proceedings*, v. 19, n. 1, pp. 112–119, 2011. doi: http://doi.org/10.2478/v10228-011-0019-7.

[13] KAMBLE, N., SONAWANE, B.U., AHUJA, B.B., "Study on forming analysis by FAB system in deep drawing process [M S2062] forming process using photogrammetric method and numerical simulation", *Journal of Machining & Forming Technologies*, v. 8, n. 1–2, pp. 41–48, 2016.

[14] TABOUROT, L., VACHER, P., COUDERT, T., *et al*., "Numerical determination of strain localiation during finite element simulation of deep drawing operations", *Journal of Materials Processing Technology*, v. 159, n. 2, pp. 152–158, 2005. doi: http://doi.org/10.1016/j.jmatprotec.2004.04.413.

[15] FEDDEMA, J.C., CHIU, L.Z.F., "Accuracy and repeatability of 3D Photogrammetry to digitally reconstruct bones", *Morphologie*, v. 108, n. 363, pp. 100793, 2024. doi: http://doi.org/10.1016/j.morpho.2024.100793. PubMed PMID: 38964273.

[16] WYJADŁOWSKI, M., KUJAWA, P., MUSZYŃSKI, Z., *et al*., "Application of photogrammetry for 3D roughness measurement of failure surface in cemented soils", *Construction & Building Materials*, v. 430, pp. 13643, 2024. doi: http://doi.org/10.1016/j.conbuildmat.2024.136431.

[17] ZHOU, L., LUO, Y., ZHANG, L., "Fast inspection of flange faces of welded tubes using photogrammetry and auxiliary measuring tools", *Measurement*, v. 237, pp. 115256, 2024. doi: http://doi.org/10.1016/j.measurement.2024.115256.

[18] TANG, H.Y., FOO, H.C.Y., TAN, I.S., *et al*., "Photogrammetry based computational fluid dynamics of erosion of sand particles in water pipeline: dynamic shape factors of 3D particles and minimization of erosion activity", *Journal of Petroleum Science Engineering*, v. 205, pp. 108794, 2021. doi: http://doi.org/10.1016/j.petrol.2021.108794.

[19] KAN, W.H., ALBINO, C., DIAS-DA-COSTA, D., *et al*., "Fracture toughness testing using photogrammetry and digital image correlation", *MethodsX*, v. 5, pp. 1166–1177, 2018. doi: http://doi.org/10.1016/j.mex.2018.09.012.

[20] CHEN, Z., LI, J., LI, T., *et al*., "RISPR/Cas212a-empowered surface plasmon, resonance platform for rapid and specific diagnosis of the Omicron variant of SARS-CoV-2", *National Science Review*, v. 9, pp. 1–10, 2022. doi: http://doi.org/10.1093/nsr/nwac104.

[21] CHEN, Z., MENG, C., WANG, X., *et al*., "Ultrasensitive DNA origami plasmon sensor for accurate detection in circulating tumor DNAs", *Laser & Photonics Reviews*, 2024. In press. doi: http://doi.org/10.1002/lpor.202400035.

[22] KOHTALA, S., ERICHSEN, J.F., WULLUM, O.P., *et al*., "Photogrammetry-based 3D scanning for supporting design activities and testing in early-stage product development", *Procedia CIRP*, v. 100, pp. 762–767, 2021. doi: http://doi.org/10.1016/j.procir.2021.05.047.

[23] TOMÁŠ, M., HUDÁK, J., DRAGANOVSKÁ, D., *et al*., "Verification of tin car body production by unconventional stamping method", *Applied Mechanics and Materials*, v. 693, pp. 364–369, 2014. doi: http://doi.org/10.4028/www.scientific.net/AMM.693.364.

[24] MUGENDIRAN, V., GNANAVELBABU, A., "Comparison of plastic strains on AA5052 by single point incremental forming process using digital image processing", *Journal of Mechanical Science and Technology*, v. 31, n. 6, pp. 2943–2949, 2017. doi: http://doi.org/10.1007/s12206-017-0537-y.

[25] PRABHARAN, T., PERIYASWAMY, P., MUGENDIRAN. V., *et al*., "Measuring deformation of deep drawing of various alloys by image processing using Matlab'', *Journal of Mines, Metals & Fuels*, v. 70, n. 10A, pp. 5–12, 2022. doi: https://doi.org/10.18311/jmmf/2022/31039.

[26] YILDIZ, R.A., YILMAZ, S., "The verification of strains obtained by grid measurements using digital image processing for sheet metal formability", *Journal of Strain Analysis for Engineering Design*, v. 52, n. 8, pp. 506–514, 2014. doi: http://doi.org/10.1177/0309324717734669.

[27] SAXENA, K.K., DAS, I.M., MUKHOPADHYAY, J., "Evaluation of bending limit curves of aluminium alloy AA6014-T4 and dual phase steel DP600 at ambient temperature", *International Journal of Material Forming*, v. 10, n. 2, pp. 221–231, 2017. doi: http://doi.org/10.1007/s12289-015-1271-6.

[28] WU, S.H., SONG, N.N., ANDRADE PIRES, F.M., *et al*., "Prediction of forming limit diagrams for materials with HCP structure", *Acta Metallurgica Sinica*, v. 28, n. 12, pp. 1442–1451, 2015. doi: http://doi.org/10.1007/s40195-015-0344-3.